Automatica 49 (2013) 2006–2016

Contents lists available at SciVerse ScienceDirect

Automatica

journal homepage: www.elsevier.com/locate/automatica

An indirect adaptive servocompensator for signals of unknown frequencies with application to nanopositioning☆

Alex Esbrook [1], Xiaobo Tan, Hassan K. Khalil

Department of Electrical and Computer Engineering, Michigan State University, East Lansing, MI 48824, USA

ARTICLE INFO

Article history:
Received 28 January 2012
Received in revised form
12 September 2012
Accepted 9 March 2013
Available online 13 May 2013

Keywords:
Adaptive systems
Servo-compensation
Frequency estimation
Microsystems: nano- and micro-technologies
Hysteresis

ABSTRACT

We propose an adaptive servocompensator utilizing frequency estimation and slow adaptation for systems subject to inputs of unknown frequencies. We show that the proposed controller can achieve zero tracking error for a class of periodic references and disturbances, including scenarios specifically relevant to piezo-actuated nanopositioning systems. In particular, for the case of a sinusoidal reference input, we establish the exponential stability of the closed-loop system in the presence of harmonic disturbances, under certain conditions on the amplitudes of the reference and disturbances. We also prove exponential stability in the case of sinusoidal reference and disturbance with two distinct frequencies. Additionally, we show that the proposed method, in conjunction with approximate hysteresis inversion, can attenuate the effect of hysteresis nonlinearity preceding linear dynamics and ensure the boundedness of the closed-loop system. Experiments conducted on a commercially available nanopositioner confirm our theoretical analysis and demonstrate the effectiveness of the proposed method as compared to Iterative Learning Control, a competitive technique in nanopositioning for tracking periodic references.

1. Introduction

The tracking problem for both linear and nonlinear systems has been a commonly explored topic in the control literature. Among the variety of techniques employed for solving such problems are servocompensators, also known as internal model controllers, which were developed for linear systems in the 1970's (Davison, 1972; Francis & Wonham, 1975). The most appealing feature of servocompensators is that, in the presence of plant uncertainty, they can completely cancel disturbances whose internal models are contained in the controller as long as the system remains stable. Isidori and Byrnes extended the internal model technique to nonlinear systems in Isidori and Byrnes (1990), and many authors have coupled servocompensators with adaptive controllers to address unknown internal models (Elliott & Goodwin, 1984; Nikiforov, 1998; Serrani, Isidori, & Marconi, 2001). The applications of internal model controllers are also diverse. For example, Isidori, Marconi, and Serrani applied an adaptive servocompensator to an altitude tracking problem in helicopters (Isidori, Marconi, & Serrani, 2003), and Singh and Schy utilized a servocompensator to control an elastic robotic arm (Singh & Schy, 1986).

Another popular topic in the literature over the past two decades has been the control of smart materials and other systems with hysteresis (Cavallo, Natale, Pirozzi, & Visone, 2003; Iyer, Tan, & Krishnaprasad, 2005; Tan & Baras, 2004; Tan & Iyer, 2009). Piezoelectric-actuated systems in particular have generated a great deal of interest due to their use in nanopositioner applications, such as Scanning Probe Microscopy (SPM) (Devasia, Eleftheriou, & Moheimani, 2007). From a theoretical perspective, an intriguing element in the control of piezo-actuated systems is dealing with the strong coupling between uncertain vibrational dynamics and the hysteresis nonlinearity (Devasia et al., 2007). In such devices, hysteresis is caused by the existence of multiple stable equilibria of the polarization state for any applied electric field (Smith, 2005), and, along with vibration and creep, it is a major obstacle impeding high-accuracy, high-speed tracking (Croft, Shed, & Devasia, 2001). Due to high performance demands in SPM applications, there are many ongoing efforts to apply advanced control techniques to nanopositioning systems. H_∞ control (Salapaka, Sebastian, Cleveland, & Salapaka, 2002) and 2-degree-of-freedom control (Lee & Salapaka, 2009) have been shown to provide robustness to plant uncertainty and facilitate tracking in the presence of hysteresis. In the work of Zhong and Yao (2008), the hysteresis effect was

☆ This work was supported by the National Science Foundation (CMMI 0824830). The material in this paper was partially presented at the 2012 American Control Conference (ACC2012), June 27–29, 2012, and the 50th IEEE Conference on Decision and Control (CDC) and the European Control Conference (ECC), December 12–15, 2011, Orlando, Florida, USA. This paper was recommended for publication in revised form by Associate Editor Andrea Serrani under the direction of Editor Miroslav Krstic.

E-mail addresses: esbrooka@msu.edu (A. Esbrook), xbtan@egr.msu.edu (X. Tan), khalil@egr.msu.edu (H.K. Khalil).

[1] Tel.: +1 2484444583; fax: +1 517 353 1980.

0005-1098/$ – see front matter © 2013 Elsevier Ltd. All rights reserved.
http://dx.doi.org/10.1016/j.automatica.2013.03.016

modeled by a combination of a linear gain and an unstructured exogenous disturbance, which was attenuated by an adaptive robust controller. Sliding mode control (Bashash & Jalili, 2009) and disturbance observers (Yang, Hara, Kanae, Wada, & Su, 2010; Yi, Chang, & Shen, 2009) have also been used to compensate for the effect of hysteresis.

An interesting approach to the control of systems with hysteresis utilizes the aforementioned servocompensators, due to their ability to facilitate high-frequency tracking while attenuating the impact of hysteresis (Esbrook, Tan, & Khalil, 2013). It is often of interest to adapt the servocompensator, so that the controller design does not require exact knowledge of the internal model and no manual modification to the controller is needed should the internal model change. However, traditional *adaptive* servocompensators, which adapt directly all internal model parameters, can struggle in systems with hysteresis. In Esbrook, Tan, and Khalil (2010) we implemented an adaptive servocompensator, based on the design described in Serrani et al. (2001), on a nanopositioning stage. Despite some initial success, the controller failed to respond properly when we attempted to compensate for harmonics of the reference. In this example, there were four parameters in the internal model, intended to compensate for the fundamental frequency and the second harmonic. After a lengthy period of slow drift, a series of peaking events occurred in the first and third adaptation variables. These issues were caused by the fact that the harmonics introduced by hysteresis are small compared to the reference; therefore, the corresponding variables have difficulty converging during adaptation.

To overcome the problems observed above, in this paper we propose augmenting an internal model regulator with a frequency-estimation-based slow adaptation law, a combination which we refer to as an *indirect adaptive servocompensator*. In this paper, the term *frequency* refers to the *fundamental frequency* of a periodic signal. For example, a sinusoid, a triangular wave, or a square wave will all be referred to as having one frequency although the latter two clearly have harmonic frequency components. Similarly, when we say two or more frequencies, we mean specifically frequencies that are not known *a priori* to be multiples of each other (thus cannot be simply treated as harmonics). When sinusoidal or sawtooth waves (a.k.a. raster or triangular waves) are passed through a hysteresis operator, the output signal possesses a spectrum with frequency components at multiples of the reference frequency (Esbrook & Tan, 2012). We can use this knowledge to design a more efficient adaptive controller. In particular, by using multiples of the estimated frequency, we are able to facilitate tracking while simultaneously attenuating the effect of hysteresis without increasing the number of adaptation variables.

In this paper, we investigate the performance and stability of the indirect adaptive servocompensator in a variety of situations. We first establish local exponential stability for the general case of n unknown frequencies. Our main theoretical results focus first on the case where the plant is subjected to a sinusoidal reference input with unknown frequency and to a disturbance consisting of the harmonics of that frequency, and we present a condition on the amplitude of the fundamental frequency component with respect to those of the harmonics that guarantee exponential stability and zero tracking error. Second, we prove exponential stability for systems subjected to a sinusoidal reference and a sinusoidal disturbance that have distinct, unknown frequencies, using a phase-portrait based approach. Based on our exponential stability results, we then extend our work to systems with hysteresis, and establish the boundedness of the closed-loop system when the adaptive servocompensator is used in conjunction with a hysteresis compensator. We finally present simulation and experimental results, which confirm our theoretical analysis and demonstrate the effectiveness of the proposed controller in nanopositioning applications. While it is not feasible to compare our proposed method with all reported approaches in nanopositioning (which are many), we have implemented an Iterative Learning Controller (ILC) (Wu & Zou, 2007), as this method is among the most competitive control schemes in nanopositioning literature, and is similarly specialized to periodic signals. We observe that the proposed method outperforms ILC for sinusoidal signals at 5, 25, 50, 100 and 200 Hz, and is competitive with ILC for a sawtooth signal of 5 Hz.

Several related problems have been addressed in the literature. In particular, both Bodson and Douglas (1997) and Brown and Zhang (2004) utilize estimation of an unknown frequency and an internal model controller to reject an unknown disturbance. Lu and Brown extended the work of Brown and Zhang (2004) to the case where the disturbance is an exponentially damped sinusoid (Lu & Brown, 2010). Wang et al. dealt with this problem in a noisy discrete-time setting, where an additional adaptive controller was included to combat the noise and minimize the output variance (Wang, Chu, & Tsao, 2009). However, each of these works focuses on the case where there is only one unknown frequency, and furthermore, do not analytically explore the case where harmonic disturbances are present.

The paper is organized as follows. In Section 2, we introduce the class of plants and signals to be considered, and also present the controller design. Stability of the system in a variety of scenarios is shown in Section 3. The performance of the closed-loop system when hysteresis inversion error is present is discussed in Section 4. Simulation and experimental results on tracking control of a nanopositioner are presented and discussed in Section 5, and concluding remarks are given in Section 6.

2. Problem formulation and controller design

We will consider systems comprised of a linear plant $G_p(s)$, represented in state-space as

$$\begin{aligned}\dot{x}(t) &= Ax(t) + B(u(t) + \alpha(t))\\ y(t) &= Cx(t)\end{aligned} \tag{1}$$

where $u(t)$ is the control signal, and $\alpha(t)$ is a matched disturbance. The control objective is to regulate the tracking error $e(t) = y_r(t) - y(t)$ to zero, where $y_r(t)$ denotes the reference signal to be tracked. We will deal with a variety of reference and disturbance signals in this paper, and the general form we consider is

$$y_r(t) = \sum_{k=1}^{m} R_{1i} \sin(\zeta_k \omega_1 t + \Phi_{1k}) \tag{2}$$

$$\alpha(t) = \sum_{i=1}^{n} \sum_{k=1}^{m} r_{ik} \sin(\zeta_k \omega_i t + \phi_{ik}) \tag{3}$$

where the frequencies ω_i, phases Φ_{1k} and ϕ_{ik}, and the amplitudes R_{1i} and r_{ik} are unknown. The constant vector $\zeta = [\zeta_1, \ldots, \zeta_m]'$ is assumed to be known *a priori* and is used in the control design. We assume that each ζ_k is a natural number, and that $\zeta_1 = 1$. Note that this class of reference signals also covers $T = 2\pi/\omega_1$-periodic waveforms approximated by a finite Fourier series. We will then focus on two special cases of (2) and (3). First, we consider a sinusoidal reference and a harmonic disturbance, which follows from the general setup by letting $n = 1$, $R_{1k} = 0, \forall k \neq 1$, and $\Phi_{11} = 0$:

$$y_r(t) = R_{11} \sin(\omega_1 t) \tag{4}$$

$$\alpha(t) = \sum_{k=1}^{m} r_{1j} \sin(\zeta_k \omega_1 t + \phi_{1k}). \tag{5}$$

This particular choice of reference and disturbance is motivated by applications such as nanopositioning (Esbrook et al., 2013), where at the steady state an input nonlinearity (e.g., hysteresis)

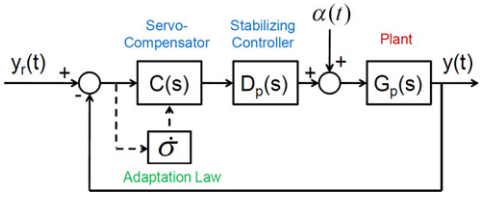

Fig. 1. Block diagram of the closed-loop system.

introduces a matched disturbance with harmonics at multiples of the frequency of a sinusoidal reference (Esbrook & Tan, 2012). The second special case of (2) and (3) we consider consists of a sinusoidal reference and sinusoidal disturbance with unknown and unrelated frequencies, i.e., $m = 1$, $n = 2$, $\Phi_{11} = 0$, and $r_{11} = 0$:

$$y_r(t) = R_{11}\sin(\omega_1 t) \tag{6}$$
$$\alpha(t) = r_{21}\sin(\omega_2 t + \phi_{21}). \tag{7}$$

This choice of reference and disturbance is indicative of a system perturbed by an external source, which is often considered in tracking problems (Isidori et al., 2003). The following assumption is typical in the servocompensator literature (Davison, 1972; Elliott & Goodwin, 1984; Francis & Wonham, 1975; Isidori & Byrnes, 1990; Nikiforov, 1998; Serrani et al., 2001).

Assumption 1. The plant $G_p(s)$ has no zero at $j\zeta_k\omega_i$, $i = 1, \ldots, n$, $k = 1, \ldots, m$.

Fig. 1 illustrates the design of the controller. First, based on the internal model principle (Davison, 1972; Francis & Wonham, 1975), we design a servocompensator for the aforementioned system. We define the servocompensator $C^i(s)$, with state $\eta^i = [\eta^i_1, \eta^i_2, \ldots, \eta^i_{2m}]' \in \mathbb{R}^{2m}$, input $e(t)$, and output $y^i_c \in \mathbb{R}$, as

$$\dot\eta^i(t) = \bar{\mathbf{C}}^*(\sigma_i)\eta^i(t) + \bar{\mathbf{B}}^* e(t) \tag{8}$$
$$y^i_c(t) = k^i_\eta(\sigma_i)\eta^i(t) + D^i_c(\sigma_i)e(t)$$

where

$$\bar{\mathbf{C}}^*(\sigma_i) = \begin{bmatrix} \zeta_1\mathbf{C}^*(\sigma_i) & \cdots & 0 \\ \vdots & \ddots & \vdots \\ \cdots & 0 & \zeta_m\mathbf{C}^*(\sigma_i) \end{bmatrix}, \qquad \bar{\mathbf{B}}^* = \begin{bmatrix} \kappa_1\mathbf{B}^* \\ \vdots \\ \kappa_m\mathbf{B}^* \end{bmatrix}$$
$$\mathbf{C}^*(\sigma_i) = \begin{bmatrix} 0 & \sigma_i \\ -\sigma_i & 0 \end{bmatrix}, \qquad \mathbf{B}^* = \begin{bmatrix} 0 \\ 1 \end{bmatrix}.$$

σ_i is the estimate of the frequency ω_i, and $\kappa = [\kappa_1, \kappa_2, \ldots, \kappa_m]' \in \mathbb{R}^m$, $\kappa_i > 0$ $\forall i$, $k^i_\eta(\sigma_i) \in \mathbb{R}^{1\times 2m}$, and $D^i_c(\sigma_i) \in \mathbb{R}$ are design parameters used to stabilize the system. In particular, we will select the design parameters $k^i_\eta(\sigma_i)$, $D^i_c(\sigma_i)$, and κ such that each $C^i(s)$ behaves like a notch filter, similar to what was done in Mojiri and Bakhshai (2004). For example, if $n = m = 1$, then

$$C^1(s) = \frac{s^2 + 2\zeta_c\zeta_1\sigma_1 s + (\zeta_1\sigma_1)^2}{s^2 + (\zeta_1\sigma_1)^2}$$

where $\zeta_c \ll 1$ is the notch parameter. This reduces the effect the compensator has on the overall phase margin of the system, which will allow us to stabilize the system over all possible frequency estimates. We have also left ζ_1 in the above equations despite our assumption that it is equal to 1, in order to make the effect of ζ_j more clear when $n, m \neq 1$. We then utilize n such servocompensators connected in parallel to realize the compensator $C(s)$ shown in Fig. 1. The i superscript is used to denote which frequency estimate $C^i(s)$ uses. Note that if there is only one unknown frequency, $C(s) = C^1(s)$. To clarify the notation, we denote the combined state of the n parallel servocompensators $C(s)$ as $\breve\eta$. We also denote the vectors of unknown frequencies and their estimates as $\omega = [\omega_1, \ldots, \omega_n]'$ and $\sigma = [\sigma_1, \ldots, \sigma_n]'$, respectively.

We will also require a stabilizing controller $D_p(s)$, given in the state-space as

$$\dot\xi(t) = A_d\xi(t) + B_d\left(\sum_{i=1}^n y^i_c(t)\right) \tag{9}$$
$$u(t) = C_d\xi(t) + D_d\left(\sum_{i=1}^n y^i_c(t)\right). \tag{10}$$

The output of the stabilizing controller $D_p(s)$ is $u(t)$, the control signal to the plant (1). We will also define the state vector $\chi = [x, \breve\eta, \xi]$ for later use. Since the frequencies are unknown, the vector $\sigma \in \Re^n$ will be updated by an adaptation law, the goal of which is to drive the parameter error $\tilde\sigma = \sigma - \omega$ to zero. The estimation of the ith frequency σ_i will be governed by the adaptation law,

$$\dot\sigma_i = -\gamma_i\sigma_i(t)e(t)\eta^i_1(t) \tag{11}$$

where $1 \gg \gamma_i > 0$ is the adaptation gain, and η^i_1 represents the first component of the state vector η^i of the servocompensator $C^i(s)$. The smallness of γ_i is required to facilitate two-time-scale averaging analysis on the system, which will be discussed in Section 3. Furthermore, we will select the initial condition of σ to be positive and bounded away from zero. The form of the adaptation law was originally derived from a formal gradient approach, then modified into that in (11) to guarantee stability. A very similar adaptation law was proposed by Brown and Zhang in Brown and Zhang (2004).

3. Analysis of the closed-loop system

We shall analyze the closed-loop system using two-time-scale averaging theory (Sastry & Bodson, 1989; Teel, Moreau, & Nesic, 2003). Two-time-scale averaging allows us to separate the analysis of the closed-loop system into the analysis of two separate subsystems, a fast or boundary-layer system, and a slow or average system. We first establish the stability of the boundary-layer system in Section 3.1. In the following subsections, we investigate the stability for the average system, and subsequently for the full closed-loop system, for different cases of the reference and disturbance input. Specifically, in Section 3.2 we prove local exponential stability for the general n-frequency case. In Sections 3.3 and 3.4, we establish stronger, global exponential stability results for more specialized cases of one frequency (4)–(5), and two frequencies (6)–(7), respectively.

3.1. Stability of the boundary-layer system

First define the matrices

$$\breve{\mathbf{C}}^*(\sigma) = \mathrm{diag}(\bar{\mathbf{C}}^*(\sigma_1), \bar{\mathbf{C}}^*(\sigma_2), \ldots, \bar{\mathbf{C}}^*(\sigma_n))$$
$$k_\eta(\sigma) = [k^1_\eta(\sigma_1)', k^2_\eta(\sigma_2)', \ldots, k^n_\eta(\sigma_n)']'$$
$$D_c(\sigma) = \sum_{i=1}^n D^i_c(\sigma_i)$$

and $\breve B^*$ as an n-high stack of vectors $\bar{\mathbf{B}}^*$. We now define the boundary-layer system for the general closed-loop system (1)–(3), (8)–(11), by setting $\gamma_i = 0, \forall i = 1, 2, \ldots, n$ in (11). This freezes the value of σ at σ_{bl}. Denoting the state variables of the boundary-layer system as $\chi_{bl} = [x'_{bl}, \breve\eta'_{bl}, \xi'_{bl}]'$, we write the closed-loop

boundary-layer system as

$$\dot{\chi}_{bl}(t) = f_{bl}(\chi_{bl}, \sigma_{bl}, t) = \begin{bmatrix} (A - BD_dD_c(\sigma_{bl})C) & BD_dk_\eta(\sigma_{bl}) & BC_d \\ -\breve{B}^*C & \breve{C}^*(\sigma_{bl}) & 0 \\ -B_dD_c(\sigma_{bl})C & B_dk_\eta(\sigma_{bl}) & A_d \end{bmatrix} \chi_{bl} + \begin{bmatrix} BD_dD_c(\sigma_{bl})y_r(t) + B\alpha(t) \\ \breve{B}^*y_r(t) \\ B_dD_c(\sigma_{bl})y_r(t) \end{bmatrix}. \quad (12)$$

Using frequency-domain techniques, we can use the stabilizing controller (9)–(10) to establish input-to-state stability (ISS) of the boundary-layer system. Recall that we have selected the output matrices of $C(s)$ to guarantee that it behaves like a notch filter. Therefore, we can design $D_p(s)$ to stabilize the transfer function

$$H_p(s) = \frac{D_p(s)G_p(s)}{1 + D_p(s)G_p(s)}. \quad (13)$$

Using this controller structure, it can be shown that the system will be ISS-stable for a small enough ζ_c, provided the gain crossover frequency ω_{gc} of $H_p(s)$ is sufficiently far away from σ_{bl}. Note that since the boundary-layer system is linear, ISS implies that the closed-loop system states will converge to the steady-state trajectories exponentially fast for any periodic reference $y_r(t)$ and disturbance $\alpha(t)$. In addition, note that if $\sigma_{bl} = \omega$, the tracking error $e(t)$ will converge to zero.

3.2. Averaging analysis for the case of n unknown frequencies: local exponential stability

We now shift our attention to the slow or average system. This analysis is based on the two-time-scale averaging framework presented in Sastry and Bodson (1989), and we will utilize this framework to analyze the closed-loop system for different reference trajectories in Sections 3.2–3.4. We begin by considering the case where there are n unknown frequencies, shown in (2) and (3). We first define θ_i as the average of σ_i, as well as the vector $\theta = [\theta_1, \ldots \theta_n]$. The dynamics of θ_i obey

$$\dot{\theta}_i = F_{av}(\chi_{bl}(\theta, t), \theta_i, t) = -\lim_{\tau\to\infty} \frac{\gamma}{\tau} \int_0^\tau \theta_i e(t)\eta_1^i(t)\, dt \quad (14)$$

where $e(t)$ and $\eta_1^i(t)$ represent the steady-state trajectories of e and η resulting from the boundary-layer system (12) with $\sigma_{bl} = \theta$. We will make the following assumption to simplify the form of the equation for the average dynamics $\dot{\theta}$.

Assumption 2. The combinations $\zeta_f\omega_i$ are unique, i.e., $\zeta_f\omega_i \neq \zeta_g\omega_k$ for all $i, k = 1, \ldots, n;, f, g = 1, \ldots, m$, unless $f = g$ and $i = k$.

This assumption implies that no two unknown frequencies share a harmonic of order below $\max(\zeta)$, and is primarily made to keep the following equations manageable. Define $G_p(s) \triangleq G_n(s)/G_d(s)$, and let

$$\bar{C}_i(s) = \prod_{k=1,k\neq i}^{n} \prod_{l=1}^{m} (s^2 + (\zeta_l\theta_k)^2) \cdot \prod_{l=2}^{m} (s^2 + (\zeta_l\theta_i)^2). \quad (15)$$

We also define

$$F_i(\zeta_l, \omega_k) = \gamma_i\theta_i^2\kappa_1|\bar{C}_i(j\zeta_l\omega_k)|^2/2 \quad (16)$$

$$D(j\zeta_l\omega_k) = G_d(j\zeta_l\omega_k)C_d(j\zeta_l\omega_k) + G_n(j\zeta_l\omega_k)C_n(j\zeta_l\omega_k)D_p(j\zeta_l\omega_k) \quad (17)$$

where $C(s) = C_n(s)/C_d(s)$. We also will require following definition,

$$H_l(j\omega_k) = \Big[R_{1l}^2|G_d(j\omega_k)|^2 + r_{1l}^2|G_n(j\omega_k)|^2 - 2R_{1l}r_{1l}|G_d(j\omega_k)| \times |G_n(j\omega_k)| \cdot \cos(\angle G_p(j\omega_k) + \Phi_{1l} + \phi_{1l})\Big]. \quad (18)$$

Note that $H_l \geq (R_{1l} - |G_p|r_{1l})^2 \geq 0$. Using Assumption 2 and the above definitions, we can calculate the form of $\dot{\theta}_i$ (derivation details omitted in the interest of brevity):

$$\dot{\theta}_i = \sum_{l=1}^{m} \frac{-F_i(\zeta_l, \omega_1)H_l(j\omega_1)(\theta_i^2 - \zeta_l^2\omega_1^2)}{|D(j\zeta_l\omega_1)|^2} + \sum_{k=2}^{n}\sum_{l=1}^{m} \frac{-F_i(\zeta_l, \omega_k)|G_n(j\zeta_l\omega_k)|^2r_{kl}^2(\theta_i^2 - \zeta_l^2\omega_k^2)}{|D(j\zeta_l\omega_k)|^2}. \quad (19)$$

Note that, for every $i, k = 1, \ldots, n$ and $l = 1, \ldots, m$ there exists a combination θ_i and $\zeta_l\omega_k$ such that $\bar{C}_i(j\zeta_l\omega_k)$ is zero if $\theta_i = \omega_k$, except for the case where $i = k$ and $l = 1$. This fact can be seen by looking at the final product grouping in (15), $\prod_{l=2}^{m}[(s^2 + (\zeta_l\theta_i)^2)]$. In addition, notice that $|\bar{C}_i(j\zeta_l\omega_k)|$ always appears squared. Therefore, using the product rule of differentiation, we can see that any partial derivative of the right-hand side of (19) with respect to $\theta_l, \forall l = 1, \ldots, n$ and evaluated at the equilibrium point $\theta = \omega$ will be zero, except the partial derivative with respect to θ_i. In addition, this guarantees that when this partial derivative is evaluated at $\theta = \omega$, only the portion of the derivative taken with respect to the term $(\theta_i^2 - \zeta_l^2\omega_k^2)$ will be non-zero. This can be calculated as

$$\left.\frac{\partial\dot{\theta}_i}{\partial\theta_i}\right|_{\theta=\omega} = \sum_{l=1}^{m} \frac{-F_i(\zeta_l, \omega_1)H_i(j\omega_1)(2\omega_i)}{|D(j\zeta_l\omega_1)|^2} + \sum_{k=2}^{n}\sum_{l=1}^{m} \frac{-F_i(\zeta_l, \omega_k)|G_n(j\zeta_l\omega_k)|^2r_{kl}^2(2\omega_i)}{|D(j\zeta_l\omega_k)|^2} \quad (20)$$

which is always negative over the adaptation variable range. Therefore, the resulting Jacobian of the average system is comprised of negative terms in the diagonal, and zeros everywhere else; thus the average system is exponentially stable for sufficiently small initial conditions $(\theta(0) - \omega)$. We also note that if $\theta = \omega$, the closed-loop system (1)–(3), (8)–(11) transformed into error coordinates possesses an equilibrium where $e(t) = 0$. Let $\bar{\chi}$ denote the steady-state solution of the aforementioned closed-loop system when $\sigma(t) \equiv \omega$. Then by Theorem 4.4.3 of Sastry and Bodson (1989), the origin of the closed-loop system with coordinates $(\chi(t) - \bar{\chi}(t), \sigma(t) - \omega)$ is locally exponentially stable.

3.3. Averaging analysis for the case of one unknown frequency: exponential stability

In this subsection, we will focus on the case where there is one unknown frequency, and present a sufficient condition for the exponential stability of the closed-loop system. We will assume that y_r and α obey (4)–(5).

Assumption 3. The plant $G_p(s)$ has no poles at $s = j\omega_1$.

Theorem 1. *Consider the closed-loop system (1), (4)–(5), and (8)–(11). Let Assumptions 1 and 3 hold. Let $\bar{\chi}$ denote the steady-state solution of the aforementioned closed-loop system when $\sigma(t) \equiv \omega_1$. Then, for all bounded initial conditions $(\chi(0), \sigma(0))$ where $\sigma(0) > 0$, there exist constants $R_r > 0$ (dependent on $\{r_{1l}\}_{l=1}^m$) and $\epsilon_\gamma > 0$, such that, if $R_{11} > R_r$ and $\gamma < \epsilon_\gamma$, all states of the closed-loop system are bounded. In addition, the origin of the closed-loop system expressed in the error coordinates $(\chi(t) - \bar{\chi}(t), \sigma(t) - \omega_1)$ is exponentially stable, and the tracking error $e(t)$ converges to zero exponentially fast.*

Proof. To prove Theorem 1, we will require exponential stability of both the boundary layer system, established through the controller design in the previous subsection, and exponential stability of the average system. Note that we will be removing the i super and subscripts from signals in this subsection, since there is only one frequency to estimate. Now let

$$\bar{C}(s) = \prod_{k=2}^{m}(s^2 + (\zeta_k\theta)^2). \tag{21}$$

We can then calculate $\dot{\theta}$ as,

$$\dot{\theta} = \frac{-F(1,\omega_1)H(j\omega_1)}{|D(j\omega_1)|^2}(\theta^2 - \omega_1^2) + \sum_{l=2}^{m}\frac{-F(\zeta_l,\omega_1)r_{1l}^2|G_n(j\zeta_l\omega_1)|^2(\theta^2 - (\zeta_l\omega_1)^2)}{|D(j\zeta_l\omega_1)|^2} \tag{22}$$

where F and H are defined by suppressing the subscripts in (16) and (18) respectively. Note that $H(j\omega_1)$ is guaranteed to be non-negative, and is positive (due to Assumptions 1 and 3) if $R_{11} > r_{11}|G_p(j\omega_1)|$, which we will assume for the remainder of our analysis. In addition, notice that $\dot{\theta}$ is positive for $\omega_1 > \theta > 0$, and negative for $\theta > \zeta_m\omega_1$; therefore the initial condition of θ defines an invariant set Σ in which θ resides for all time. We now use Lyapunov analysis to show exponential stability of the average system. We start with the Lyapunov function candidate $V = \tilde{\theta}^2/2$, where $\tilde{\theta} = \theta - \omega_1$. Using (22) and the definition of $H(j\omega_1)$, we can evaluate $\dot{V}$ as

$$\dot{V} = \frac{-F(1,\omega_1)H(j\omega_1)(\theta+\omega_1)}{|D(j\omega_1)|^2}\tilde{\theta}^2 + \sum_{l=2}^{m}\frac{-F(\zeta_l,\omega_1)r_{1l}^2|G_n(j\zeta_l\omega_1)|^2(\theta^2 - (\zeta_l\omega_1)^2)}{|D(j\zeta_l\omega_1)|^2}\tilde{\theta}. \tag{23}$$

It can be easily seen from (23) that if $r_{1l} = 0, \forall l > 1$, there will exist a constant $k > 0$ such that $\dot{V} \le -kV$. This proves exponential stability of the system if $\alpha(t) = 0$.

We now focus on the case where $r_{1l} \neq 0$. It is important to note that $|\bar{C}(j\zeta_l\omega_1)|$, and thus $F(\zeta_l,\omega_1)$, possesses a term of the form $|\zeta_l\theta - \zeta_l\omega_1| = \zeta_l|\tilde{\theta}|$. Also note that $(\theta^2 - (\zeta_l\omega_1)^2)$ and $\tilde{\theta}$ possess the same sign when $\theta < \omega_1$ or $\theta > \zeta_m\omega_1$. This implies that there exists a constant $c_1 > 0$ such that $\dot{V} \le -c_1V$ when $\tilde{\theta} \notin [0, \zeta_m\omega_1 - \omega_1]$. We can therefore focus our attention on the set $\tilde{\theta} \in [0, \zeta_m\omega_1 - \omega_1]$. We notice that within this set, $|\tilde{\theta}| = \tilde{\theta}$. Therefore, when $l \neq 1$, we can find a constant $c_f > 0$ to bound $F(\zeta_l,\omega_1)$ in the set $\tilde{\theta} \in [0, \zeta_m\omega_1 - \omega_1]$ as

$$F(\zeta_l,\omega_1) \le c_f\tilde{\theta}.$$

Finally, from (22) and the condition $R_{11} > r_{11}|G(j\omega_1)|$, H is strictly increasing with the reference amplitude R_{11}, while $F(\cdot)$ is independent of R_{11}. This allows us to write, for positive constants k_1 and k_2,

$$\dot{V} \le -R_{11}^2k_1\tilde{\theta}^2 + c_fk_2\tilde{\theta}^2 \tag{24}$$

where the existence of k_1 and k_2 are guaranteed by the boundedness of θ within the set of interest. Therefore, for a sufficiently large R_{11}, there exists a constant $c_2 > 0$ such that when $\tilde{\theta} \in [0, \zeta_m\omega_1 - \omega_1]$,

$$\dot{V} \le -c_2V. \tag{25}$$

Since both c_1 and c_2 are greater than zero, we can use the minimum of these two constants to bound $\dot{V}$ for all $\tilde{\theta}$, and conclude the exponential stability of the average system. Since we have now shown exponential stability of both the average and boundary layer trajectories, we can apply Theorem 4.4.3 of Sastry and Bodson (1989), and conclude exponential stability of the trajectory $(\bar{\chi}, \omega_1)$ for a sufficiently small adaptation gain γ, which also implies the boundedness of the state trajectory and the convergence of the tracking error to zero. □

Remark 1. Assumption 3 is not typically found in the adaptive control literature; however, it is required in our proof since Theorem 1 shows both the tracking error e and adaptation error $\tilde{\theta}$ converge to zero. If this assumption is not satisfied, stability can still be shown for sufficiently large r_{11} by using r_{11} in the same manner R_{11} was used in the above proof. This is because if $G_d(j\omega_1) = 0$, from (18), $H(j\omega_1)$ becomes $r_{11}^2|G_n(j\omega_1)|^2$.

Remark 2. The required size of $R_{11} > R_r$ is determined by the sizes of the constants k_1 and k_2 in (24). These constants vary with the frequency ω_1, plant transfer function $G_p(s)$, stabilizing controller $D_p(s)$, and the size of the disturbance.

3.4. Averaging analysis for the case of two unknown frequencies: exponential stability

We now present results on the stability of the closed-loop system in the case of two unknown frequencies, (6)–(7). Without loss of generality, we will assume for our analysis that $\omega_1 < \omega_2$. We will also set $\gamma_1 = \gamma_2 = \gamma$, which will create a very useful symmetry in the dynamics of the average system. As there are now multiple frequency estimates, we will reintroduce the i subscript in order to differentiate between the first and second frequency estimates and frequencies. Using the symmetry of the system, we can compute the dynamics of the average system as

$$\begin{aligned}\dot{\theta}_1 &= f(\theta_1,\theta_2)\\ \dot{\theta}_2 &= f(\theta_2,\theta_1)\end{aligned} \tag{26}$$

where

$$f(a,b) = \frac{-\mathbb{F}(a,b,\omega_1)R_{11}^2|G_d(j\omega_1)|^2(a^2-\omega_1^2)}{|\mathbb{D}(a,b,\omega_1)|^2} + \frac{-\mathbb{F}(a,b,\omega_2)r_{21}^2|G_n(j\omega_2)|^2(a^2-\omega_2^2)}{|\mathbb{D}(a,b,\omega_2)|^2} \tag{27}$$

$$\mathbb{F}(a,b,\omega_i) = \gamma a^2\kappa_1(b^2-\omega_i^2)^2/2 \tag{28}$$

$$\begin{aligned}\mathbb{D}(a,b,\omega_i) = {} & G_d(j\omega_i)(a^2-\omega_i^2)(b^2-\omega_i^2)\\ & + [G_n(j\omega_i)D_p(j\omega_i)(a^2-\omega_i^2+2\zeta\omega_iaj)\\ & \cdot(b^2-\omega_i^2+2\zeta\omega_ibj)]\end{aligned} \tag{29}$$

where due to the symmetry of the system, we note that $\mathbb{D}(a,b,\omega_i) = \mathbb{D}(b,a,\omega_i)$. We will analyze the system (26) using a phase portrait approach. Based on the terms $(a^2-\omega_1^2)$ and $(a^2-\omega_2^2)$ in (27), we know that the system possesses equilibrium points at $\theta = (\omega_1,\omega_2)$ and $\theta = (\omega_2,\omega_1)$. Because of the symmetric structure of the controller, either of these equilibrium points is desirable from a tracking perspective, as the boundary layer system at either point possess zero tracking error. A second consequence of the terms $(a^2-\omega_1^2)$ and $(a^2-\omega_2^2)$ is that, from any positive initial condition θ_0, the state θ enters the invariant set $(\theta_1,\theta_2) \in [\omega_1,\omega_2]\times[\omega_1,\omega_2] \triangleq \Omega$. This follows from the inequalities $\mathbb{F}(a,b,\omega_i) > 0, \forall a < \omega_1, i = 1,2$ and $\mathbb{F}(a,b,\omega_i) < 0, \forall a > \omega_2, i = 1,2$. Within Ω, we have the following result.

Lemma 1. *Let Assumptions 1 and 3 hold. For any $\theta \in \Omega$, the inner product*

$$\left\langle \begin{bmatrix}\dot{\theta}_1\\ \dot{\theta}_2\end{bmatrix}, \begin{bmatrix}-1\\ 1\end{bmatrix}\right\rangle$$

is positive if $\theta_2 > \theta_1$, negative if $\theta_2 < \theta_1$, and zero if $\theta_2 = \theta_1$, except for the cases $\theta = (\omega_1, \omega_2)$ or $\theta = (\omega_2, \omega_1)$, where the inner product is zero.

Proof. The inner product can be directly calculated as

$$\begin{aligned}\left\langle \begin{bmatrix}\dot\theta_1\\ \dot\theta_2\end{bmatrix}, \begin{bmatrix}-1\\ 1\end{bmatrix}\right\rangle &= f(\theta_1,\theta_2) - f(\theta_2,\theta_1)\\ &= \frac{\gamma\kappa_1 R_{11}^2 |G_d(j\omega_1)|^2(\theta_1^2-\omega_1^2)(\theta_2^2-\omega_1^2)}{2|\mathbb{D}(\theta_1,\theta_2,\omega_1)|^2}\\ &\quad\cdot[\theta_1^2(\theta_2^2-\omega_1^2)-\theta_2^2(\theta_1^2-\omega_1^2)]\\ &\quad+\frac{\gamma\kappa_1 r_{11}^2 |G_n(j\omega_2)|^2(\theta_1^2-\omega_2^2)(\theta_2^2-\omega_2^2)}{2|\mathbb{D}(\theta_1,\theta_2,\omega_2)|^2}\\ &\quad\cdot[\theta_1^2(\theta_2^2-\omega_2^2)-\theta_2^2(\theta_1^2-\omega_2^2)]. \end{aligned} \tag{30}$$

The bracketed terms can be simplified to $[\omega_1(\theta_2^2-\theta_1^2)]$ and $[\omega_2(\theta_2^2-\theta_1^2)]$ respectively, which together with Assumptions 1 and 3 completes the proof. □

There are several consequences of this lemma. The first consequence is that there are no equilibrium points within the interior of Ω, except for on the line $\theta_1 = \theta_2$. However, any equilibrium points on the line must be unstable, since the vector field always points away from the $\theta_1 = \theta_2$ line inside Ω. Second, there are no possible limit cycles within Ω, as the existence of a limit cycle would require the above inner product to be zero on locations other than the $\theta_1 = \theta_2$ line. These facts, together with the forward invariance of Ω, imply that from any initial condition θ_0, the trajectory $\theta(t)$ converges to either (ω_1, ω_2) or (ω_2, ω_1). Furthermore, it can be shown that the points (ω_1, ω_2) or (ω_2, ω_1) are locally exponentially stable. We start from the Lyapunov function candidate

$$V(\theta) = \frac{(\theta_1-\omega_1)^2}{2} + \frac{(\theta_2-\omega_2)^2}{2} \triangleq \frac{\tilde\theta_1^2}{2} + \frac{\tilde\theta_2^2}{2}.$$

Consider the set

$$\Delta \triangleq \{\theta : |\tilde\theta_1| < \epsilon_c, |\tilde\theta_2| < \epsilon_c\}. \tag{31}$$

We will now show exponential stability of the point (ω_1, ω_2) within Δ. Exponential stability of the point (ω_2, ω_1) can be shown by redefining $\tilde\theta_1 = \theta_1 - \omega_2$ and $\tilde\theta_2 = \theta_2 - \omega_1$, and altering the following equations accordingly. We seek to find an ϵ_c such that $\dot V$ is negative definite within Δ. Assuming that the system is currently within the set Δ, we substitute $\theta_1 = \omega_1 + \tilde\theta_1$ and $\theta_2 = \omega_2 + \tilde\theta_2$ where $\tilde\theta_1, \tilde\theta_2 \in [-\epsilon_c, \epsilon_c]$. Using these substitutions together with (26), we can then bound $\dot V$ by

$$\begin{aligned}\dot V \le{}& \frac{-\tilde\theta_1^2 R_{11}^2\kappa_1}{|\mathbb{D}(\theta_1,\theta_2,\omega_1)|^2}[\gamma_1\theta_1^2|G_d(j\omega_1)|^2 - \gamma_2\theta_2^2|2\omega_1+\epsilon_c|\epsilon_c]\\ &+\frac{-\tilde\theta_2^2 r_{21}^2\kappa_1}{|\mathbb{D}(\theta_1,\theta_2,\omega_2)|^2}[\gamma_2\theta_2^2|G_n(j\omega_2)|^2 - \gamma_1\theta_1^2|2\omega_2+\epsilon_c|\epsilon_c]. \end{aligned} \tag{32}$$

Using Assumptions 1 and 3, we can see that for a sufficiently small ϵ_c, there exists a $c_0 > 0$ such that $\dot V \le -c_0 V$. Combining the asymptotic stability and local exponential stability, we imply from Theorem 4.4.3 of Sastry and Bodson (1989) that the origin of the closed-loop system with coordinates $(\chi(t) - \bar\chi(t), \sigma(t) - \omega)$, where $\omega = (\omega_1, \omega_2)$ or $\omega = (\omega_2, \omega_1)$, is exponentially stable. We have thus proved the following theorem.

Theorem 2. *Consider the closed-loop system (1), (6)–(11). Let Assumptions 1 and 3 hold. Let $\bar\chi$ denote the steady state solution of the aforementioned closed-loop system when $\sigma(t) \equiv \omega$, where $\omega = (\omega_1, \omega_2)$ or $\omega = (\omega_2, \omega_1)$. Then, there exists a sufficiently small γ, such that, for all bounded initial conditions $(\chi(0), \sigma(0))$ where $\sigma(0) > 0$ and $\sigma_1(0) \neq \sigma_2(0)$, all states of the closed-loop system are bounded. In addition, the origin of the closed-loop system with coordinates $(\chi(t) - \bar\chi(t), \sigma(t) - \omega)$ is exponentially stable. Furthermore, the tracking error $e(t)$ converges to zero.*

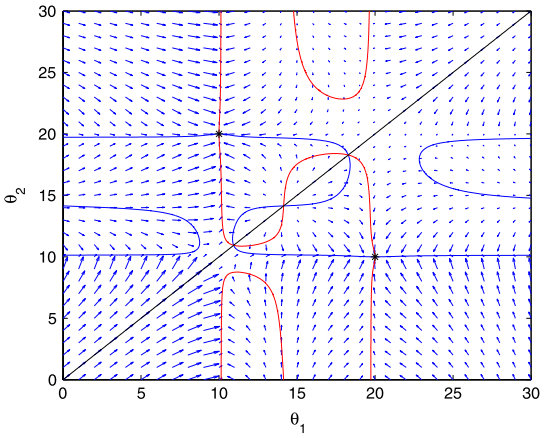

Fig. 2. Phase portrait of average system for a sample plant and controller. The zero level curves of $\dot\theta_1$ (primarily vertical) and $\dot\theta_1$ (primarily horizontal) together with the neutral axis $\theta_1 = \theta_2$ are also plotted.

Remark 3. If the initial conditions and controller parameters of each $C_i(s)$ and $\dot\sigma_i$ are chosen to be equal, the system will behave as if it is a single controller with a single adaptation law, as there will then be identical compensators connected in parallel with identical states. We refer to this as a degenerative state for the controller. This can be prevented by choosing $\sigma_1(0) \neq \sigma_2(0)$.

Remark 4. For systems with non-equal adaptation gains, it can be quickly shown that all possible equilibria in Ω, other than (ω_1, ω_2) and (ω_2, ω_1), must reside on the $\theta_1 = \theta_2$ line, and the set of these equilibria is the same as that for the case of identical adaptation gains. In addition, it can be shown that the stability properties of those equilibria are the same given different choices of adaptation gains. In other words, no stable equilibria exist in Ω except the desired points (ω_1, ω_2) and (ω_2, ω_1). However, the existence of limit cycles in this system cannot be excluded as readily as in the identical gain case, and this will be addressed in our future work.

Fig. 2 shows an example phase portrait of the average system (26). In addition to the phase portrait, we have plotted the level curves of the $\dot\theta_1$ and $\dot\theta_2$ equations. For this particular set of system parameters, there are three unstable equilibria on the $\theta_1 = \theta_2$ axis (two saddle points and one unstable node). For this special case of equal adaptation gains, the regions of attraction for the stable points can be explicitly calculated and are divided by the $\theta_1 = \theta_2$ line. For cases where the adaptation gains are not equal, the form of the regions of attraction are more complicated.

4. Analysis of the closed-loop system in the presence of hysteresis

Of particular importance to our work is the case where the matched disturbance α is the result of error in hysteresis inversion and where the reference trajectory is a sinusoid, as was the case in Esbrook et al. (2013). Consider a linear plant preceded by a Preisach-like hysteresis operator such as the Prandtl–Ishlinskii (PI) operator (Brokate & Sprekels, 1996), as illustrated in Fig. 3. Such models have proven effective at capturing the dynamics of systems with hysteresis, including piezoelectric systems (Croft et al., 2001; Devasia et al., 2007; Wu & Zou, 2007). The output of such operators are formed through a weighted superposition, i.e., $u(t) = \vartheta' W(t)$, where the elements of the vector $W(t) \in \Re^w$ are the states of

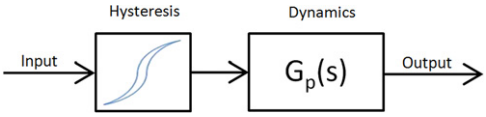

Fig. 3. Illustration of linear plant preceded by hysteresis operator, commonly used to model piezoelectric-actuated nanopositioners.

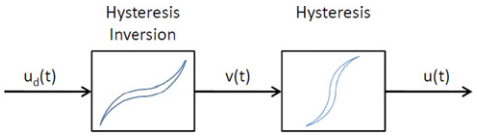

Fig. 4. Hysteresis inversion process. u_d is the desired input.

smaller hysteresis elements called hysterons, and $\vartheta \in \Re^w$ are the weights. The weights are in general unknown, so controllers must be designed based on an approximate output, $\hat{\vartheta}'W(t)$. A common and effective technique in the control of such systems is to use an inverse hysteresis operator to attenuate the effect of hysteresis (Cavallo et al., 2003; Iyer & Tan, 2009; Tao & Kokotovic, 1995), a process which is illustrated in Fig. 4. For a Presiach-like operator, one can calculate the difference between the desired input $u_d(t)$ and actual input to the linear plant $u(t)$ as (Esbrook et al., 2013)

$$u_d(t) - u(t) = \tilde{\vartheta}'W(t) \tag{33}$$

where $\tilde{\vartheta} = \hat{\vartheta} - \vartheta$. For a sinusoidal reference, we can then describe the resulting closed-loop system via equations (1), (4), (8)–(11), and (33), where we set $u_d(t)$ equal to $u(t)$ in (10). Such a system can, under suitable conditions, be shown to possess a unique, asymptotically stable T-periodic solution (Pokrovskii & Brokate, 1998; Tan & Khalil, 2009).

Once we have established that the solutions of closed-loop system are periodic at the steady state, we can use the properties of the servocompensator to analyze its disturbance attenuation properties. Since all signals in the closed-loop system are T-periodic, we can rewrite $\tilde{\vartheta}'W(t)$ using Fourier series expansion as two signals; α, which has the form of the disturbance (5), and α_d, which has the form

$$\alpha_d(t) = \sum_{l,l\notin\zeta} r_{1l}\sin(l\omega_1 t + \phi_l).$$

Here $\zeta \in \mathbb{R}^m$ will be considered as a design parameter to determine how many harmonics of the reference are compensated by the servocompensator. Therefore, we can treat the closed-loop system with hysteresis as the closed-loop system considered in Section 3.3 perturbed by the additional matched disturbance α_d. Define $X = [(\chi - \bar{\chi})', \sigma - \omega]'$ as the state vector of the nominal closed-loop system (1), (4), (8)–(11), transformed into error coordinates. We have already shown that this system is exponentially stable; therefore, from the converse Lyapunov theorem (Khalil, 2002), we have that

$$c_1\|X\|^2 \le V(X) \le c_2\|X\|^2$$
$$\dot{V} \le -c_3\|X\|^2, \qquad \left\|\frac{\partial V}{\partial X}\right\| \le c_4\|X\|$$

for a positive definite function V and positive constants $c_1, \ldots, c_4$. Now consider the closed-loop system with the disturbance α_d. Taking a time derivative of $V(X)$, we arrive at,

$$\dot{V} \le -c_3\|X\|^2 + c_4\|X\| \times \sum_{k,k\notin\zeta}^{\infty} |C_{\eta_1}(s)S(s)G_p(s)||S(s)G_p(s)|r_{1k}^2\Big|_{s=jk\omega_1}. \tag{34}$$

The RHS of (34) is negative definite for

$$\|X\| > \frac{c_4\sum_{k,k\notin\zeta}^{\infty} |C_{\eta_1}(s)S(s)G_p(s)||S(s)G_p(s)|r_{1k}^2}{c_3}\Bigg|_{s=jk\omega_1}.$$

Since $r_{1k}, \forall k \notin \zeta$ is proportional to $\|\tilde{\vartheta}'\|$, for a sufficiently small $\|\tilde{\vartheta}'\|$ and γ, there exists a constant k_3 such that $\|X\| \le k_3$. By varying the analysis above slightly, we can arrive at a similar bound for the system without hysteresis (i.e. $\alpha(t) \equiv 0$), but the reference signal is an infinite summation of sinusoids, such as a raster or triangle wave. In such a case,

$$\dot{V} \le -c_5\|X\|^2 + c_6\|X\|\sum_{k,k\notin\zeta}^{\infty} |C_{\eta_1}(s)S(s)||S(s)|R_{1k}^2\Big|_{s=jk\omega_1}$$

for some positive constants c_5 and c_6, and R_{1k} represents the amplitude of the kth harmonic component in the reference.

5. Simulation and experimental results

In this section, we present simulation and experimental results that illustrate and support the analytical results in Sections 3 and 4. Specifically, in Section 5.1, we show simulation results that demonstrate the influence of reference amplitude on the convergence for the case of one unknown frequency. Sections 5.2 and 5.3 contain experimental results that deal with the cases of one and two unknown frequencies, respectively. These experimental results also provide direct support for the analysis in Section 4, because of the presence of hysteresis compensation error in the experimental system.

5.1. Simulation results for the case of one unknown frequency

We begin by verifying the analysis presented in Section 3.3, in particular the restriction on the size of R_{11}. Recall that in order to prove stability of the closed-loop system (1), (4)–(5), and (8)–(11), we required the reference amplitude R_{11} to be sufficiently large relative to the size of the harmonic disturbances present in the system. In order to verify this, we present Fig. 5, which shows the results of a pair of simulations conducted on the vibrational model of our piezoelectric nanopositioner,

$$\dot{x}(t) = 1.0\times10^4\begin{bmatrix}-0.014 & 1.700 & 0.095 & -0.050\\ -1.700 & -0.241 & -0.672 & 0.170\\ 0.095 & 0.672 & -1.066 & 1.617\\ 0.050 & 0.170 & -1.617 & -0.305\end{bmatrix}x(t) + \begin{bmatrix}27.8\\ 111.3\\ -116.5\\ -44.1\end{bmatrix}u(t)$$
$$y(t) = \begin{bmatrix}27.8 & -111.3 & -116.5 & 44.1\end{bmatrix}x(t) \tag{35}$$

where

$$y_r(t) = R_{11}\sin(\omega_1 t)$$
$$\alpha(t) = 5\sin(2\omega_1 t)$$

$\omega_1 = 2\pi 100$, and R_{11} is a constant variable. The servocompensator was designed accordingly with $\zeta = [1, 2]$. The stabilizing controller $D(s)$ was designed using frequency-domain techniques based on the frequency response of the plant, and was chosen as

$$D_p(s) = \frac{1.3(3.5\times10^3)^2}{s^2 + 1.6(3.5\times10^3)s + (3.5\times10^3)^2}. \tag{36}$$

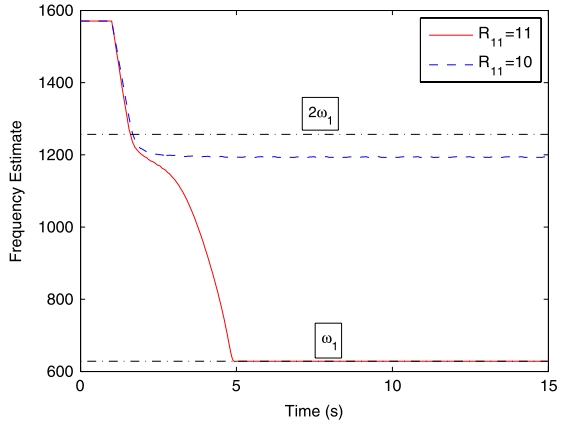

Fig. 5. Simulation results on the model of the piezoelectric plant. Two simulations are presented, with $R_{11} = 10$ and $R_{11} = 11$.

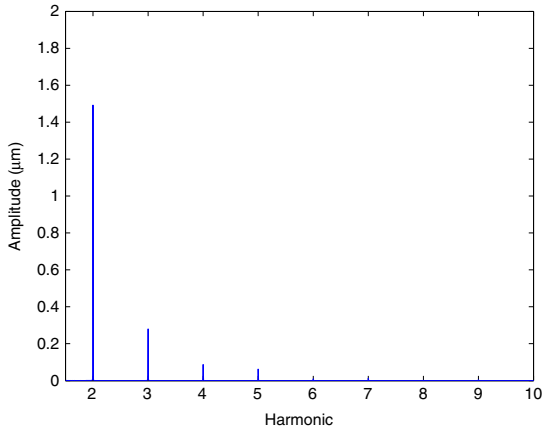

Fig. 6. Output spectrum for nanopositioner used in experimental studies. Input to power supply is $3\sin(2\pi 5) + 4V$. Primary harmonic is not shown, but has an amplitude of 25.2 μm.

This controller was verified to stabilize the boundary layer system (12) over the working range of our adaptation variable σ. When the reference amplitude $R_{11} = 11$, we notice that the frequency estimate converges to the desired value of ω_1. However, when the reference amplitude $R_{11} = 10$, the frequency estimate settles slightly below $2\omega_1$. This also results in a very large difference in tracking error, with essentially zero tracking error ($O(10^{-10})$) when $R_{11} = 11$, but 2.45 when $R_{11} = 10$; thus our results from Section 3.3 are confirmed, with the value of R_r lying somewhere between 10 and 11.

5.2. Experimental results for the case of one unknown frequency

We will now experimentally demonstrate the effectiveness of the proposed controller on a commercial piezo-actuated nanopositioner (Nano OP-65, from Mad City Labs), whose vibration dynamics are given by (35) with a primary resonance of 3 kHz. The hysteresis nonlinearity of the plant was identified using a quasi-static waveform of decreasing amplitude. A least-squares optimization routine was used to identify optimal weights for a modified PI operator (Kuhnen, 2003) with 9 deadzone elements and 8 play operators, which was then used to calculate an approximate hysteresis inversion. Fig. 6 shows the magnitude spectrum of the positioner output with a sinusoidal input. Note that the amplitude of the harmonic terms is significantly lower than that of the primary term. After inversion is implemented in the closed-loop system, these harmonic terms will be smaller; therefore we can expect the controller to stabilize the system according to Theorem 1.

Table 1
Tracking error results for proposed controllers (MHASC, ASC) and ILC. Results are presented as a percentage of the reference amplitude (20 μm).

Hz	MHASC Mean	(%) Peak	ASC Mean	(%) Peak	ILC Mean	(%) Peak
5	0.12	0.64	0.31	0.92	0.17	0.78
25	0.14	0.71	0.37	1.01	0.19	0.58
50	0.21	0.93	0.46	1.14	0.53	1.01
100	0.39	1.61	0.56	1.76	0.53	1.25
200	0.94	3.12	0.79	3.33	1.36	3.49

We tested the regulation performance of the proposed method through tracking experiments, using sinusoidal references from 5 to 200 Hz, along with a 5 Hz sawtooth signal. In order to understand the effectiveness of the proposed controller, we will compare the tracking results with an established method in nanopositioning tracking problems, Iterative Learning Control (Wu & Zou, 2007), which, like the servocompensator, is specifically suited for periodic references and effective at compensating for hysteresis effects as well as uncertain dynamics. Our performance metrics will be the mean tracking error, defined as the mean of $|e(t)|$ at steady state, and the peak tracking error, defined by computing max $|e(t)|$ over one period of the reference, then taking an average of this value over many periods.

For the sinusoidal references, we will employ two versions of our proposed controller; an indirect adaptive servocompensator (ASC) with the design vector $\zeta = [1]$, and a multi-harmonic indirect adaptive servocompensator (MHASC) with $\zeta = [1, 2, 3]$. Both controllers are based on the analysis of Section 3.3. The adaptation gains used were $\gamma = 0.003$ for the 5 and 25 Hz cases, $\gamma = 0.001$ for 50 Hz, and $\gamma = 0.0005$ for the 100 and 200 Hz experiments, where we have adjusted the adaptation gains to get similar settling times for each test.

The tracking results are presented in Table 1. We notice that the MHASC enjoys a consistent advantage over both the ILC controller and ASC controller. As the frequency of the reference trajectory increases, the ASC begins to overtake the ILC controller in performance, but is significantly behind at low frequency, indicating that the proposed controller's tracking performance is less sensitive to model uncertainties than ILC. At 200 Hz, we notice that the ASC has better mean-error performance than the MHASC, which is highly counter-intuitive. However, this can be explained by the design of the stabilizing controller. With a frequency of 200 Hz, the successive harmonics used in the MHASC mean that the servocompensator has a great effect on the stability margin of the system. For the ASC, with $\sigma = 2\pi 200$, the closed-loop system possesses a phase margin of around 70°. However, the phase margin of the MHASC at this frequency is 25°. This causes the other harmonics of the hysteresis being amplified, and results in the higher tracking error.

Figs. 7 and 8 offer a closer look at the performance of the different methods at high and low frequencies. As the system approaches the gain crossover frequency near the resonant frequency of the plant, the effect of the hysteresis harmonics are amplified, resulting in the effect of the hysteresis becoming more pronounced. We can clearly observe the more prominent presence of higher harmonics in the 100 Hz signal as compared to the 5 Hz signal.

The second reference we test is a 5 Hz sawtooth signal, with the results shown in Fig. 9. We set the design parameter $\zeta = [1, 3, 5, 7, 9, 11]$ in order to approximate for the sawtooth signal, as well as compensate hysteresis. The frequency of the sawtooth wave was limited to 5 Hz, due to concerns with the stabilizing controller. The ILC controller's wide bandwidth nature makes it much better suited to compensating a sawtooth signal than our proposed method, and this results in an mean tracking error of 0.17% for ILC versus 0.28% for our proposed controller. However, the proposed method is still able to effectively compensate the sawtooth signal.

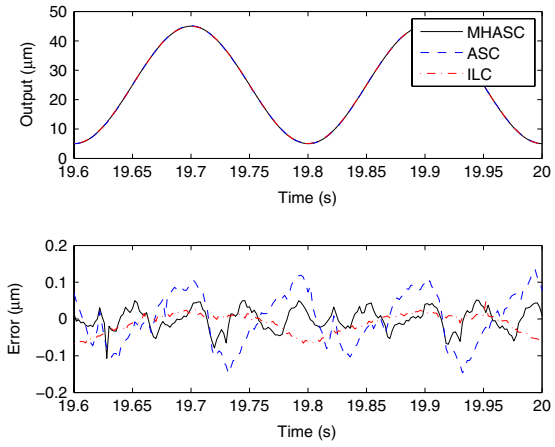

Fig. 7. Experimental results for a 5 Hz sinusoidal signal.

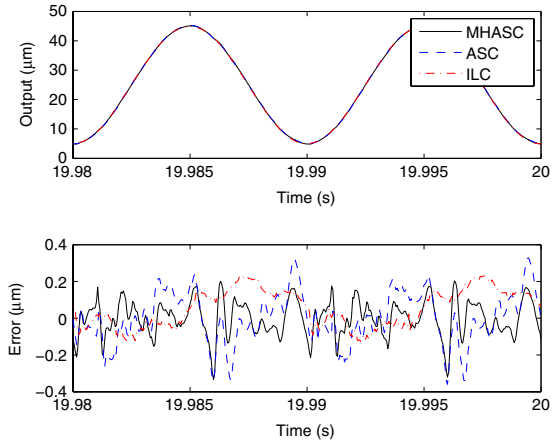

Fig. 8. Experimental results for a 100 Hz sinusoidal signal.

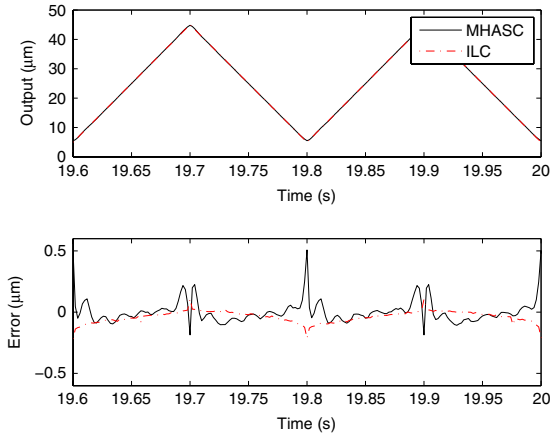

Fig. 9. Experimental results for a 5 Hz sawtooth signal.

5.3. Experimental results for the case of two unknown frequencies

We now present our experimental results on the performance of the proposed controller when y_r and α obey (6)–(7), as considered in Section 3.4. In order to simulate disturbances of the form in (7), we inject a disturbance of $10\sin(2\pi 75t+\pi/2)$ into our Simulink block diagram just before the hysteresis inversion. The reference trajectory is $10\sin(2\pi 25t)$. For the purposes of control

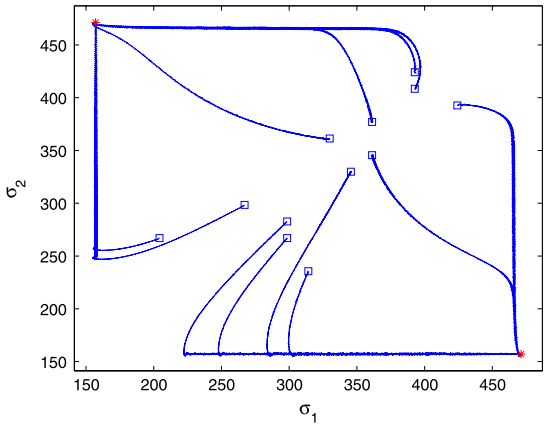

Fig. 10. Phase portrait of σ_1 and σ_2 for various initial conditions. Desired equilibria are marked by the stars (red, in the lower right and top left), and initial conditions are marked by squares.

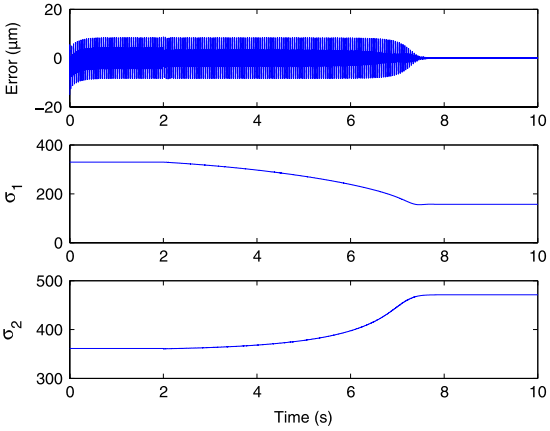

Fig. 11. Plot of tracking error and adaptation variables vs. time. Adaptation is enabled at 2 s.

design, it is assumed that both frequencies are unknown, and in particular are not treated as known multiples of each other. The adaptation gains used were $\gamma_1 = \gamma_2 = 0.001$.

Fig. 10 shows the phase portrait of the adaptation variables for a number of initial conditions. Notice that the neutral line $\sigma_1 = \sigma_2$ is not crossed in any of the experiments. The trajectories of the adaptation variables seem to indicate the presence of three unstable equilibria on the neutral line; two saddles points near the top right and lower left of the figure, and an unstable node in the center of the figure. The trajectories of the system tend to initially converge to a manifold on which one variable is close to a desired frequency, seen in Fig. 10 as the horizontal and vertical lines. The system then evolves along this manifold to the stable equilibria. The time evolution of the tracking error and adaptation variables for one set of initial conditions is shown in Fig. 11. After the adaptation is enabled at 2 s, the adaptation variables converge shortly after 7 s, which correlates with a rapid decrease in the tracking error. These experiments show the robustness of the proposed method to the error in hysteresis compensation.

6. Concluding remarks

We have presented a series of results on an indirect adaptive servocompensator motivated by nanopositioning applications. Novel analysis has been used to show that under certain conditions, exponential stability can be established for the cases

where there are one unknown frequency with a finite number of harmonics, as well when there are two unknown frequencies without harmonics. Local stability was also shown for cases with n unknown frequencies. Ultimate boundedness has been shown for the case where a linear plant cascaded with hysteresis is preceded by an inexact hysteresis inversion. In particular, we are able to show that the proposed controller can directly reduce the effect of hysteresis by compensating for the harmonics generated by hysteresis. Theoretical results are confirmed experimentally, and the controller is shown to be effective when compared to Iterative Learning Control.

Preliminary simulations seem to indicate that it is possible to extend the results for an n frequency case to include stability in the large. Analysis of this case will be addressed in future work. In addition, we plan on investigating alternative stabilizing controllers to improve the performance of the MHASC at high frequencies.

References

Bashash, S., & Jalili, N. (2009). Robust adaptive control of coupled parallel piezo-flexural nanopositioning stages. *IEEE/ASME Transactions on Mechatronics*, *14*, 11–20.

Bodson, M., & Douglas, S. C. (1997). Adaptive algorithms for the rejection of sinusoidal disturbances with unknown frequency. *Automatica*, *33*(12), 2213–2221.

Brokate, M., & Sprekels, J. (1996). *Hysteresis and phase transitions*. New York: Springer-Verlag.

Brown, L. J., & Zhang, Q. (2004). Periodic disturbance cancellation with uncertain frequency. *Automatica*, *40*(4), 631–637.

Cavallo, A., Natale, C., Pirozzi, S., & Visone, C. (2003). Effects of hysteresis compensation in feedback control systems. *IEEE Transactions on Magnetics*, *39*(3), 1389–1392.

Croft, D., Shed, G., & Devasia, S. (2001). Creep, hysteresis, and vibration compensation for piezoactuators: atomic force microscopy application. *Journal of Dynamic Systems, Measurement, and Control*, *123*(1), 35–43.

Davison, E. J. (1972). The output control of linear time-invariant multivariable systems with unmeasurable arbitrary disturbances. *IEEE Transactions on Automatic Control*, *17*(5), 621–630.

Devasia, S., Eleftheriou, E., & Moheimani, S. O. R. (2007). A survey of control issues in nanopositioning. *IEEE Transactions on Control Systems Technology*, *15*, 802–823.

Elliott, H., & Goodwin, G.C. (1984). Adaptive implementation of the internal model principle. In *Proceedings of the 23rd IEEE conference on decision and control* (pp.1292–1297).

Esbrook, A., & Tan, X. (2012). Harmonic analysis for hysteresis operators with application to control design for systems with hysteresis. In *Proceedings of the 2012 American control conference* (pp. 1652–1657).

Esbrook, A., Tan, X., & Khalil, H. (2010). A robust adaptive servocompensator for nanopositioning control. In *49th IEEE conference on decision and control* (pp. 3688–3693).

Esbrook, A., Tan, X., & Khalil, H. K. (2013). Control of Systems With hysteresis via servocompensation and its application to nanopositioning. *IEEE Transactions on Control Systems Technology*, *21*(3), 725–738.

Francis, B., & Wonham, W. (1975). The internal model principle for linear multivariable regulators. *Applied Mathematics and Optimization*, *2*, 170–194.

Isidori, A., & Byrnes, C. I. (1990). Output regulation of nonlinear systems. *IEEE Transactions on Automatic Control*, *35*(2), 131–140.

Isidori, A., Marconi, L., & Serrani, A. (2003). Robust nonlinear motion control of a helicopter. *IEEE Transactions on Automatic Control*, *48*(3), 413–426.

Iyer, R., & Tan, X. (2009). Control of hysteretic systems through inverse compensation: inversion algorithms, adaptation, and embedded implementation. *IEEE Control Systems Magazine*, *29*(1), 83–99.

Iyer, R., Tan, X., & Krishnaprasad, P. (2005). Approximate inversion of the Preisach hysteresis operator with application to control of smart actuators. *IEEE Transactions on Automatic Control*, *50*(6), 798–810.

Khalil, H. K. (2002). *Nonlinear systems* (3rd ed.). Upper Saddle River, NJ: Prentice Hall.

Kuhnen, K. (2003). Modeling, identification and compensation of complex hysteretic nonlinearities—a modified Prandtl–Ishlinskii approach. *European Journal of Control*, *9*(4), 407–418.

Lee, C., & Salapaka, S. M. (2009). Fast robust nanopositioning: a linear-matrix-inequalities-based optimal control approach. *IEEE/ASME Transactions on Mechatronics*, *14*(4), 414–422.

Lu, J., & Brown, L. J. (2010). Internal model principle-based control of exponentially damped sinusoids. *International Journal of Adaptive Control and Signal Processing*, *24*(3), 219–232.

Mojiri, M., & Bakhshai, A. R. (2004). An adaptive notch filter for frequency estimation of a periodic signal. *IEEE Transactions on Automatic Control*, *49*(2), 314–318.

Nikiforov, V. (1998). Adaptive nonlinear tracking with complete compensation of unknown disturbances. *European Journal of Control*, *4*, 132–139.

Pokrovskii, A. V., & Brokate, M. (1998). Asymptotically stable oscillations in systems with hysteresis nonlinearities. *Journal of Differential Equations*, *150*, 98–123.

Salapaka, S., Sebastian, A., Cleveland, J. P., & Salapaka, M. V. (2002). High bandwidth nano-positioner: a robust control approach. *Review of Scientific Instruments*, *73*(9), 3232–3241.

Sastry, S., & Bodson, M. (1989). *Adaptive control: stability, convergence, and robustness*. Englewood Cliffs, NJ: Prentice Hall.

Serrani, A., Isidori, A., & Marconi, L. (2001). Semiglobal nonlinear output regulation with adaptive internal model. *IEEE Transactions on Automatic Control*, *46*(8), 1178–1194.

Singh, S., & Schy, A. (1986). Elastic robot control: nonlinear inversion and linear stabilization. *IEEE Transactions on Aerospace and Electronic Systems*, *AES-22*(4), 340–348.

Smith, R. C. (2005). *Smart material systems*. Philadelphia, PA: Society for Industrial and Applied Mathematics [Online]. Available http://link.aip.org/link/doi/10.1137/1.9780898717471.

Tan, X., & Baras, J. S. (2004). Modeling and control of hysteresis in magnetostrictive actuators. *Automatica*, *40*(9), 1469–1480.

Tan, X., & Iyer, R. (2009). Modeling and control of hysteresis: introduction to the special section. *IEEE Control Systems Magazine*, *29*(1), 26–29.

Tan, X., & Khalil, H.K. (2009). Two-time-scale averaging of systems involving operators and its application to adaptive control of hysteretic systems. In *Proceedings of the 2009 American control conference* (pp. 4476–4481).

Tao, G., & Kokotovic, P. V. (1995). Adaptive control of plants with unknown hystereses. *IEEE Transactions on Automatic Control*, *40*(2), 200–212.

Teel, A. R., Moreau, L., & Nesic, D. (2003). A unified framework for input-to-state stability in systems with two time scales. *IEEE Transactions on Automatic Control*, *48*(9), 1526–1544.

Wang, Y., Chu, K., & Tsao, T.-C. (2009). Adaptive rejection of stochastic and deterministic sinusoidal disturbances with unknown frequency. In *Proceedings of the 2009 American control conference* (pp. 5641–5646).

Wu, Y., & Zou, Q. (2007). Iterative control approach to compensate for both the hysteresis and the dynamics effects of piezo actuators. *IEEE Transactions on Control Systems Technology*, *15*(5), 936–944.

Yang, Z.-J., Hara, S., Kanae, S., Wada, K., & Su, C.-Y. (2010). An adaptive robust nonlinear motion controller combined with disturbance observer. *IEEE Transactions on Control Systems Technology*, *18*(2), 454–462.

Yi, J., Chang, S., & Shen, Y. (2009). Disturbance-observer-based hysteresis compensation for piezoelectric actuators. *IEEE/ASME Transactions on Mechatronics*, *14*(4), 454–462.

Zhong, J., & Yao, B. (2008). Adaptive robust precision motion control of a piezoelectric positioning stage. *IEEE Transactions on Control Systems Technology*, *16*, 1039–1046.

Alex Esbrook received the Bachelors of Science degree in Electrical Engineering from Michigan State University, East Lansing MI, USA, in 2008. Since May 2008, he has been a member of the Smart Microsystems Laboratory in the Department of Electrical and Computer Engineering at Michigan State University. His research interests include control of systems with hysteresis, regulation theory, adaptive systems, automotive control, and collaborative control. Mr. Esbrook received an award for best session presentation at the 2010 American Control Conference, and an honorable mention for the 2009 National Science Foundation graduate research fellowship.

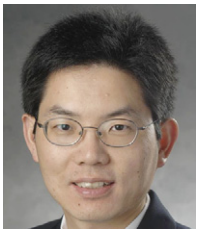

Xiaobo Tan received the B.Eng. and M.Eng. degrees in Automatic Control from Tsinghua University, Beijing, China, in 1995 and 1998, respectively, and the Ph.D. degree in Electrical and Computer Engineering from the University of Maryland, College Park, in 2002.

From September 2002 to July 2004, he was a Research Associate with the Institute for Systems Research at the University of Maryland. He joined the faculty of the Department of Electrical and Computer Engineering at Michigan State University (MSU) in 2004, where he is currently an Associate Professor. His current research interests include modeling and control of smart materials, electroactive polymer sensors and actuators, biomimetic robotic fish, mobile sensing in aquatic environments, and collaborative control of autonomous systems. Dr. Tan is keen to integrate his research with educational and outreach activities, and currently leads an NSF-funded Research Experiences for Teachers (RET) Site on Bio-Inspired Technology and Systems (BITS) at MSU.

Dr. Tan is an Associate Editor of Automatica and a Technical Editor of IEEE/ASME Transactions on Mechatronics. He served as the Program Chair for the 15th International Conference on Advanced Robotics (ICAR 2011). He was a Guest Editor of IEEE Control Systems Magazine for its February 2009 issue's Special Section on Modeling and Control of Hysteresis. Dr. Tan received the NSF CAREER Award in 2006, the 2008 ASME DSCD Best Mechatronics Paper Award (with Yang Fang) in 2009, and the Teacher-Scholar Award from MSU in 2010.

Hassan K. Khalil received the B.S. and M.S. degrees in Electrical Engineering from Cairo University, Egypt, in 1973 and 1975, respectively, and the Ph.D. degree from the University of Illinois, Urbana-Champaign, in 1978, all in Electrical Engineering.

Since 1978, he has been with Michigan State University (MSU), where he is currently University Distinguished Professor of Electrical and Computer Engineering. He has consulted for General Motors and Delco Products, and published several papers on singular perturbation methods and nonlinear control. He is the author of Nonlinear Systems (Macmillan 1992; Prentice Hall 1996 & 2002) and coauthor of *Singular Perturbation Methods in Control: Analysis and Design* (Academic Press 1986; SIAM 1999).

Dr. Khalil was named an IFAC Fellow in 2007. He received the 1989 IEEE-CSS George S. Axelby Outstanding Paper Award, the 2000 AACC Ragazzini Education Award, the 2002 IFAC Control Engineering Textbook Prize, the 2004 AACC O. Hugo Schuck Best Paper Award, and the 2009 AGEP Faculty Mentor of the Year Award. At MSU he received the 2003 Teacher Scholar Award, the 1994 Withrow Distinguished Scholar Award, and the 1995 Distinguished Faculty Award. He served as Associate Editor of the IEEE TRANSACTIONS ON AUTOMATIC CONTROL, *Automatica*, and *Neural Networks*, and as Editor of *Automatica* for nonlinear systems and control. He was Registration Chair of the 1984 CDC, Finance Chair of the 1987 ACC, Program Chair of the 1988 ACC, and General Chair of the 1994 ACC.